PAPER • OPEN ACCESS

Collective effects in emission of localized excitons strongly coupled to a microcavity photon

To cite this article: A N Poddubny *et al* 2013 *New J. Phys.* **15** 025016

View the article online for updates and enhancements.

New Journal of Physics

Collective effects in emission of localized excitons strongly coupled to a microcavity photon

A N Poddubny[1], M M Glazov and N S Averkiev

Ioffe Physical-Technical Institute of the RAS, St Petersburg 194021, Russia
E-mail: poddubny@coherent.ioffe.ru

Abstract. A theory of nonlinear emission of localized excitons coupled to the optical mode of the microcavity is presented. Numerical results are compared with analytical ones. The effects of exciton–exciton interaction within the quantum dots and with the reservoir formed by non-resonant pumping are considered. It is demonstrated that the nonlinearity due to the interaction strongly affects the shape of the emission spectra. The collective superradiant mode of the excitons is shown to be stable against the nonlinear effects.

Contents

[1] Author to whom any correspondence should be addressed.

IOP Institute of Physics **⚛** DEUTSCHE PHYSIKALISCHE GESELLSCHAFT

1. Introduction

Semiconductor quantum dots are often referred to as 'artificial atoms' owing to their discrete energy spectrum. The progress in nanotechnology has made it possible to employ quantum dots as a *sui generis* solid-state laboratory for studies of quantum mechanics [1, 2]. Interband optical pumping of quantum dots gives rise to electron–hole pairs or zero-dimensional excitons, which, as shown in the pioneering works [3–5], can strongly couple with the photon trapped in the optical microcavity. The strong coupling effect results in a coherent energy transfer between the photon and the exciton; this phenomenon is widely studied for bulk materials and planar quantum well structures [6–9]. Its observation in zero-dimensional systems has attracted an enormous excitement among the research community, since the concepts of quantum electrodynamics were directly transferred to the solid state. Such quantum-dot-in-a-cavity systems demonstrate fascinating fundamental physics [10–13] and may be advantageous for quantum optics device applications [12, 14–16].

The physical concept of the strong coupling in zero-dimensional microcavities can be easily understood considering, as an example, two classical pendulums with close frequencies of oscillations ω_1 and ω_2 connected by a spring, which induces the coupling between the pendulums of a strength g. One of these oscillators represents a photon, the other one stands for an exciton, and the spring describes radiative recombination of the exciton into the photon mode. If the dampings of the individual oscillators are small compared with the coupling constant, the eigenfrequencies ω of this interacting system follow from the simple equation

$$(\omega - \omega_1)(\omega - \omega_2) = g^2 \tag{1}$$

as

$$\omega_\pm = \frac{\omega_1 + \omega_2}{2} \pm \sqrt{\left(\frac{\omega_1 - \omega_2}{2}\right)^2 + g^2}. \tag{2}$$

The normal modes correspond to the coupled oscillations: by exciting one pendulum one eventually excites another, so the energy is transferred back and forth between them.

The analogy between the quantum electrodynamical problem of the quantum dot exciton interacting with the microcavity photon and the purely classical problem of two coupled pendulums is quite deep. The excitonic polarization in a semiconductor is indeed described by the oscillator-like equation of motion and so is the electric field of the cavity photon [1, 8]. Hence, the physics of these two different systems is similar, which greatly simplifies the theoretical description of quantum-dot-in-a-cavity dynamics [17, 18]. The situation becomes particularly interesting if $N > 1$ dots are placed in the microcavity: it turns out that, provided the dots are identical, only one excitonic mode—termed *superradiant* (or bright)—interacts with the cavity mode, and the interaction constant is enhanced compared with that in one dot by the factor $\sqrt{N}$. In classical language, for N pendulums describing quantum dot excitons, one oscillation mode is specific, namely, the mode where all pendulums oscillate in phase with each other.

Just like the classical oscillators which are ideal only as far as model situations are considered, the excitons and photons interact with the environment, which gives rise to their damping and dephasing; moreover, the oscillation law can differ from the harmonic one. The main reasons for anharmonicity are identified: interactions between excitons lead to their energy shifts, the oscillator strength saturation results in the decrease of the coupling constant

with an increase of the exciton number in the system, excitons can bind together to form biexcitons [1, 19]. Hence, the analysis of the nonlinear dynamics of the quantum dot excitons strongly coupled to the cavity mode is of prime importance. In particular, the stability of the superradiant mode with respect to the interactions should be investigated.

In this paper, we consider the simplest possible and physically most transparent case of the nonlinearity caused by the exciton–exciton interaction in large quantum dots or quantum boxes. It is analogous to the cubic anharmonicity of the pendulum. We calculate the optical emission spectra of the quantum-dot-in-a-cavity system under a non-resonant excitation (photoluminescence spectra). The non-resonant pumping is modeled as a random force acting on the corresponding oscillator [18, 20]. The parameter which controls the nonlinearity is the pumping rate: the higher the pumping, the larger the fluctuations of excitonic polarization and, correspondingly, the higher the nonlinear terms in the equations of motion.

In this approach, the exciton state is described as a classical anharmonic oscillator. Hence, this approach is valid for large enough quantum dots (or boxes) where excitons are quantized as a whole, i.e. where exciton localization length is larger than the Bohr radius. A similar behavior can be expected in a variety of systems, including mesoscopic semiconductor structures with planar quantum microcavities where excitons can be trapped by the disorder and the nonlinear regime is easily reached [21, 22], quantum well structures with dipolar excitons [23, 24], as well as many others, e.g. optomechanical structures where the optical mode of the cavity interacts with a classical oscillator [25]. The effects of the oscillator strength saturation are related to the two-level nature of exciton transition in a small quantum dot. These effects were considered in [26–28] and are beyond the scope of the present paper.

This paper is organized as follows. Section 2 outlines the model, section 3 is devoted to the role of the reservoir fluctuations, and section 4 presents the study of the nonlinearity due to the exciton interaction. The main results are summarized in section 5.

2. The model

For distinctness, we consider here a zero-dimensional microcavity where one or several quantum dots (boxes) are embedded. We suppose that the energy (or frequency, we put $\hbar = 1$ for brevity) spacing between the cavity modes is large enough to consider only one relevant photonic mode whose frequency ω_C is close enough to frequencies of optical transitions in quantum dots $\omega_{X,i}$, $i = 1, \ldots, N$, where N is the dot number. For simplicity, only the interaction of the cavity mode with the ground states of quantum dot excitons is considered; the treatment can be generalized to allow for the excited states. Moreover, the polarization degree of freedom of the cavity mode and spin degrees of freedom of excitons are disregarded. Under these approximations the equations of motion for the dimensionless electric field E and excitonic polarizations P_i can be written as

$$\frac{\mathrm{d}E}{\mathrm{d}t} = -\left(\mathrm{i}\omega_C + \frac{\Gamma_C}{2}\right)E - \mathrm{i}g\sum_i P_i,$$

$$\frac{\mathrm{d}P_i}{\mathrm{d}t} = -\left(\mathrm{i}\omega_{X,i} + \frac{\Gamma_{X,i}}{2} + \mathrm{i}\alpha_i|P_i|^2 + \mathrm{i}\beta_i n_R\right)P_i - \mathrm{i}gE + f_i(t), \quad i = 1, \ldots, N. \tag{3}$$

Here Γ_C and $\Gamma_{X,i}$ are (phenomenological) decay rates for the cavity and excitons, respectively, g is the light–matter coupling constant (taken to be the same in all dots for the sake of simplicity).

Its evaluation is beyond the present work; rigorously it can be done by solving Maxwell equations and the Schrödinger equation for the exciton envelope functions in quantum dots, see [29–31]. Even in the absence of nonlinearities, $\alpha_i = 0$, $\beta_i = 0$, equation (3) demonstrates that the interaction of excitons with the photonic mode induces a coupling between different excitonic states. Such a radiative interaction has been studied previously for microcavity systems [17, 18, 32, 33] and for quantum dots without a cavity [34–38].

Equation (3) for exciton polarization also contains nonlinear and driving terms. The former ones, proportional to the interaction parameters $\alpha_i > 0$, describe the blueshifts of excitonic states due to interactions within the same dot. Here and further, we assume that the quantum dot (box) size is comparable to or larger than excitonic Bohr radius to accommodate several excitons in the dot [26]. Another possibility is to consider a planar microcavity structure with a lateral potential confining the exciton, see, e.g., [39]. Terms $\propto \beta_i n_R$ take into account the interaction of quantum dot excitons with a reservoir formed, e.g., by excitons and electron–hole pairs within the wetting layer. The reservoir population n_R is, in general, a function of the pumping intensity W and exciton occupations, $n_R \equiv n_R(W, |P_1|^2, \ldots, |P_N|^2)$. Driving terms described by random forces f_i, $\langle f_i \rangle = 0$ account for the exciton generation in quantum dots caused by their relaxation from the wetting layer and excited states, see [18, 20] for details. These random forces represent the white noise

$$\langle f_i(t) f_j^*(t') \rangle = S_i \delta_{ij} \delta(t - t'), \tag{4}$$

characterized by the exciton generation rate S_i proportional to the reservoir population, $S_i = s_i n_R$, where s_i is related to the relaxation rate of excitons toward the ground state [18]. In what follows, we assume that higher-order correlators of random forces are reduced to the second-order ones, equation (4), in accordance with the Gaussian distribution. Such random forces model the incoherent non-resonant pumping of our system. Similar approaches were used to study optical emission of exciton–polaritons in Bragg multiple quantum well structures and for planar microcavities [20, 40–42].

We are ultimately interested in the luminescence spectrum given (up to the common factor) by [18]

$$I(\omega) = \langle |E(\omega)|^2 \rangle = \int_{-\infty}^{\infty} \langle E(t + t') E^*(t) \rangle e^{i\omega t'} \, dt', \tag{5}$$

where averaging over time t is assumed. If the nonlinear contributions are disregarded, the emission spectrum can be obtained analytically with the result [18]:

$$I_{\text{lin}}(\omega) = \sum_{m,m'=1}^{N+1} \frac{C_{\text{cav}}^{(m)*} C_{\text{cav}}^{(m')} \sum_{i=1}^{N} C_i^{(m)*} S_i C_i^{(m')}}{(\Omega_m^* - \omega)(\Omega_{m'} - \omega)}. \tag{6}$$

Here, Ω_m are the eigenfrequencies of the homogeneous system (3) found neglecting nonlinear terms $\propto \alpha_i$, β, i.e. Ω_m are the polariton frequencies, and $[C_{\text{cav}}^{(m)}, C_1^{(m)}, \ldots, C_N^{(m)}] \equiv [E, P_1, \ldots, P_N]$ are the corresponding eigenvectors, i.e. the Hopfield coefficients of the excitonic polaritons formed by the excitons coupled to the cavity mode [8]. The spectrum equation (6) can also be recast as a sum of terms with poles at polariton frequencies Ω_m, Ω_m^*.

The detailed analysis of equation (6) is presented in [18]. Here, we briefly discuss an important liming case where all exciton frequencies are the same, $\omega_{X,1} = \omega_{X,2} = \cdots = \omega_{X,N} \equiv \omega_X$, exciton decay rates are the same, $\Gamma_{X,1} = \Gamma_{X,2} = \cdots = \Gamma_{X,N} \equiv \Gamma_X$ and the decay rates are negligible compared with the coupling constants, $\Gamma_X, \Gamma_C \ll g$. Under these assumptions the

IOP Institute of Physics Φ DEUTSCHE PHYSIKALISCHE GESELLSCHAFT

polariton frequencies and Hopfield coefficients take a simple form. There are two mixed modes with the frequencies, cf equation (2),

$$\Omega_{1,2} = \frac{\omega_X + \omega_C}{2} - i\frac{\Gamma_X + \Gamma_C}{4} \pm \sqrt{\left(\frac{\omega_X - \omega_C}{2}\right)^2 + Ng^2}, \qquad (7)$$

and all the remaining $N-1$ modes correspond to the exciton states decoupled from light, $\Omega_m = \omega_X$ for $m = 3, \ldots, N+1$. The effective coupling strength is enhanced by the factor $\sqrt{N}$ due to the formation of the collective mode: dipole moments of excitons oscillate in phase. Correspondingly, the emission spectrum has two peaks at Ω_1 and Ω_2 split by $2\sqrt{N}g$:

$$I_{\text{lin}}(\omega) \equiv \langle |E(\omega)|^2 \rangle \propto \frac{1}{|(\omega - \omega_X + i\Gamma_X/2)(\omega - \omega_C + i\Gamma_C/2) - Ng^2|^2}. \qquad (8)$$

We note that equation (8) is valid even if the condition $\Gamma_X \ll g$ or $\Gamma_C \ll g$ is violated [18]. Two distinct peaks are observed in the emission spectra for the broadenings as high as $\Gamma_X, \Gamma_C \sim \sqrt{N}g$; otherwise these two peaks merge into one.

   We now turn to the discussion of the nonlinear effects. Firstly, we consider interactions with the reservoir described by the terms $\propto \beta_i n_R P_i$; afterwards, we discuss the effects of exciton–exciton interaction within the same dot described by the terms $\propto \alpha_i |P_i|^2 P_i$.

3. Interaction with a reservoir

Under conventional non-resonant pumping conditions the excitons are generated in the wetting layer and form a reservoir. If the pumping rate is moderate the majority of excitons are in the reservoir and its occupation is only weakly affected by the presence of the quantum dots; hence, one can treat n_R in equation (3) as an independent quantity. For the steady-state pumping $\langle n_R \rangle = \bar{n}_R$ and there are certain fluctuations of δn_R around this time-averaged value, $\delta n_R = n_R - \bar{n}_R$.

   To elucidate the role of the reservoir, we neglect completely the nonlinearities caused by the exciton–exciton interaction in quantum dots, i.e. we put $\alpha_i \equiv 0$ in equation (3). It is instructive to analyze the case of a single quantum dot and disregard the light–matter interaction. In this situation, we obtain

$$\frac{dP}{dt} = -\left(i\omega_X + \frac{\Gamma_X}{2} + i\beta\bar{n}_R + i\beta\delta n_R\right)P + f(t). \qquad (9)$$

For clarity we have separated in equation (9) the contributions due to the mean number of particles in a reservoir and due to its fluctuations. Equation (9) is the first-order linear differential equation which can be integrated with the result

$$P(t) = \int_0^t dt' f(t') \exp\left[-(i\omega_X + i\beta\bar{n}_R + \Gamma_X/2)(t - t') - i\beta \int_{t'}^t \delta n_R(t'')dt''\right],$$

where the solution of the homogeneous equation is omitted. The autocorrelation function $\langle P(t)P^*(0) \rangle$, whose Fourier transform determines the single dot emission spectrum in the case of the regime of weak coupling with the photon, reads

$$\langle P(t)P^*(0) \rangle = \frac{S}{\Gamma_X}\left\langle \exp\left[-i\omega_X t - \frac{\Gamma_X t}{2} - i\beta\bar{n}_R - i\beta \int_0^t \delta n_R(t_1)dt_1\right]\right\rangle. \qquad (10)$$

Here the averaging over the random source realizations and reservoir population is assumed. The fluctuations of the reservoir particle number n_R take place on a much longer timescale compared with the fluctuations of random forces, equation (4). Hence, the averaging over the realizations of f is carried out independently.

The oscillation spectrum, $\langle |P(\omega)|^2 \rangle = \int_{-\infty}^{\infty} \langle P(t) P^*(0) \rangle \mathrm{d}t$, which corresponds to the quantum dot emission spectrum in the weak coupling regime, depends strongly on the relation between various timescales in the system: the exciton lifetime $1/\Gamma_X$, correlation time in the reservoir τ_c, defined by the relation $\langle \delta n_R(t) \delta n_R(0) \rangle = \langle \delta n_R^2 \rangle \mathrm{e}^{-t/\tau_c}$, and dephasing time τ_d caused by the reservoir, where

$$\frac{1}{\tau_d} = \beta^2 \int_0^{\infty} \mathrm{d}t \, \langle \delta n_R(t) \delta n_R(0) \rangle = \beta^2 \langle \delta n_R^2 \rangle \tau_c. \tag{11}$$

If reservoir fluctuations are fast and small enough, $\tau_c \ll \tau_d, \Gamma_X^{-1}$, the so-called motional narrowing regime can be realized and

$$\langle |P^2(\omega)| \rangle \propto \frac{1}{(\omega - \omega_X - \beta \bar{n}_R)^2 + [\Gamma_X/2 + 1/(2\tau_d)]^2}. \tag{12}$$

In this case, interactions with a reservoir slightly broaden the quantum dot spectrum.

In the opposite case, where the fluctuations are strong and slow, the quantum dot spectrum can be presented as

$$\langle |P(\omega)|^2 \rangle \propto \int \mathrm{d}n_R \, p(n_R) \delta(\omega - \omega_X - \beta n_R) = \beta^{-1} p\left(\frac{\omega - \omega_X}{\beta}\right), \tag{13}$$

where $p(n_R)$ is the distribution function of the reservoir, i.e. the probability that the number of particles in the reservoir is n_R. The quantum dot spectrum equation (13) in the regime of strong fluctuations reflects the distribution of particles in the reservoir. Equation (13) is valid for the frequencies $|\omega - \omega_X - \beta \bar{n}_R| \gtrsim \Gamma_X$; that is why the spectral function of the quantum dot is replaced by δ-function in equation (13). This equation also holds provided that the particle number fluctuations in the reservoir are so large that

$$\beta \sqrt{\langle \delta n_R^2 \rangle} \gg \Gamma_X, \quad \tau_c^{-1}. \tag{14}$$

In this case, dephasing takes place at a timescale $\sim (\beta \sqrt{\langle \delta n_R^2 \rangle})^{-1}$ and it is not sensitive either to the oscillator lifetime or to the correlation time of the reservoir.

These two limiting cases of reservoir fluctuations described by equations (12) and (13) are illustrated in figure 1(a) where the calculated quantum dot spectra are shown. The black/dashed curve presents the spectrum for vanishing reservoir fluctuations; this spectrum is described by the Lorentzian with the FWHM equal to Γ_X, centered at the resonance frequency ω_X. The blue/dotted curve corresponds to the regime of fast reservoir fluctuations, equation (12). This spectrum is also a Lorentzian, shifted to larger energies and broadened as compared with the linear regime. The red/solid curve is calculated in the regime of slow reservoir fluctuations. We have assumed that the reservoir population is characterized by a Gaussian distribution with given mean value $\bar{n}_R$ and dispersion δn_R. In numerical calculations the δ-function in equation (13) was replaced by the Lorentzian with FWHM equal to Γ_X. Then the convolution (13) yields a Voigt distribution with a Gaussian-like central part and Lorentzian wings, see figure 1(a).

It is noteworthy that for the quantum dot placed in the microcavity, the emission spectrum in the limit of weak and fast fluctuations, $\tau_c \ll \tau_d, \Gamma_X^{-1}$ is given by equation (6) where ω_X is
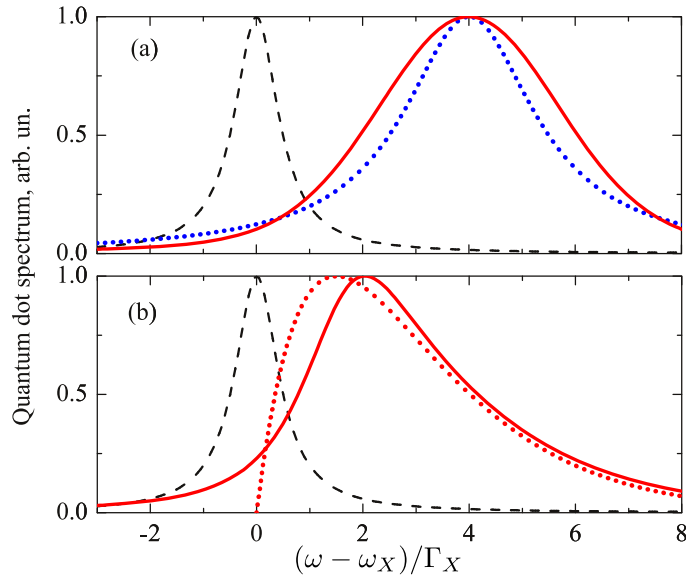
Figure 1. Effect of interaction with the reservoir (a) and within the quantum dot (b) on its spectrum $\langle |P(\omega)|^2 \rangle$. Black/dashed, red/solid and blue/dotted curves in panel (a) correspond to the linear regime, the fast reservoir fluctuations regime and the regime of slow reservoir fluctuations with Gaussian statistics, respectively. Calculation was performed at $\beta \bar{n}_R = 4\Gamma_X$, $1/\tau_d = 2\Gamma_X$ and $\beta \delta \bar{n}_R = 1.5\Gamma_X$. Black/dashed, red/solid and red/dotted curves in panel (b) correspond to the linear regime, exact solution, equation (23) and approximate solution equation (22), with δ-function replaced by the Lorentzian with full-width at half-maximum (FWHM) equal to Γ_X. Calculation was performed at $\alpha S = 3\Gamma_X$.

replaced by $\omega_x + \beta \bar{n}_R$ and Γ_X is replaced by $\Gamma_X + \tau_d^{-1}$. The qualitative shape of the spectra in the case of strong or slow reservoir fluctuations can be obtained by the convolution of the reservoir distribution function $p(n_R)$ with equation (6) where ω_X is substituted by $\omega_X + \beta n_R$. The resulting spectra are similar to those discussed in section 4.2 where the case of nonlinearity within the dot is addressed.

4. Interaction within the same dot

Now we focus on the nonlinear effects due to the interaction of the excitons within the same quantum dot. Hereinafter we will disregard fluctuations of the particles in the reservoir studied in section 3. Below we present one after another the studies of (i) the single dot case (section 4.1), (ii) a single dot coupled with the cavity mode (section 4.2) and (iii) two quantum dots coupled with the cavity (section 4.3).

4.1. A single dot

A physical picture of the interaction effects within the dot on the emission spectra can be most transparently presented for the case of a single quantum dot which does not interact with the photon. Similarly to the situation studied in section 3, its spectral function $\langle |P(\omega)|^2 \rangle$ defines the emission spectrum in the weak coupling regime.

We start with the equation describing the quantum dot as a nonlinear oscillator:

$$\frac{dP}{dt} = -\left(i\omega_X + i\alpha|P|^2 + \frac{\Gamma_X}{2}\right)P + f(t), \quad \langle f(t)f^*(t')\rangle = S\delta(t-t'). \tag{15}$$

Similarly to the case of reservoir fluctuations, equation (9), the interaction term in equation (15) leads to a blueshift and broadening of the oscillation spectrum. Consequently, analysis of reservoir fluctuations, performed above, may be used here. The strength of the fluctuating nonlinear term is determined by the value of pumping. A large pumping $(\alpha\langle|P|^2\rangle \gg \Gamma_X)$ corresponds to the regime of strong fluctuations, cf equation (14). Hence, the quantum dot spectrum may be presented in the form, similar to equation (13),

$$\langle|P(\omega)|^2\rangle = \int d\Omega F(\Omega)\delta(\Omega - \omega), \tag{16}$$

where the distribution function $F(\Omega)$ with the oscillator frequency $\Omega = \omega_X + \alpha|P|^2$ is determined from the statistics of the nonlinear term in equation (15).

A major difference between the nonlinear equation (15) and the linear equation (9) describing the interaction of the quantum dot exciton with the reservoir is that the fluctuations of the polarization P themselves govern the blueshift and, on the other hand, the blueshift determines the fluctuations of P. In order to determine the distribution function $F(\Omega)$, we use the stochastic linearization of equation (15) described in detail in [43, 44]. The starting point of the stochastic linearization is the time-dependent equation (15) where decay and pumping terms are neglected, $\Gamma_X \equiv 0$, $f(t) \equiv 0$. The solution of equation (15) is then given by $P(t) = |P|\,e^{-i\Omega t}$, where

$$\Omega|P|^2 = \omega_X|P|^2 + \alpha|P|^4. \tag{17}$$

In the presence of decay and pumping, equation (17) does not hold. In the stochastic linearization approach, the difference of the left- and right-hand sides of equation (17) should be minimized. It implies, in particular, that the average (over the random sources realizations) blueshift of the resonance frequency is given by

$$\langle\Omega - \omega_X\rangle = \frac{\alpha\langle|P|^4\rangle}{\langle|P|^2\rangle}. \tag{18}$$

Hereinafter, we use the notation $\langle|P|^2\rangle \equiv \langle|P(t=0)|^2\rangle = \int d\omega\langle|P(\omega)^2|\rangle/(2\pi)$. Equation (18) is automatically satisfied when the distribution of the frequency Ω is chosen of the form

$$F(\Omega) = \mathcal{N}(\Omega - \omega_X)p\left(\frac{\Omega - \omega_X}{\alpha}\right), \tag{19}$$

where $\mathcal{N}$ is the normalization constant,

$$p(|P|^2) = \frac{1}{\langle|P|^2\rangle}\exp\left(-\frac{|P|^2}{\langle|P|^2\rangle}\right) \tag{20}$$

is the distribution function of the exciton polarization absolute value and

$$\langle|P^2|\rangle = \frac{S}{\Gamma_X} \tag{21}$$

is given by the ratio of the pumping and decay rates. The shape of this distribution is independent of the pumping rate. In other words, the nonlinear term in equation (15) influences the oscillator phase only and does not affect its amplitude. Thus, the distribution equation (20) is the same as

that in the linear regime and inherits the Gaussian statistics of the noise term fluctuations. Using equations (18) and (20), we find that

$$\langle |P(\omega)|^2 \rangle \propto F(\omega) = \begin{cases} (\omega - \omega_X) \exp\left(-\dfrac{\omega - \omega_X}{\alpha \langle |P^2| \rangle} \right), & \omega > \omega_X, \\ 0, & \omega < \omega_X. \end{cases} \tag{22}$$

This function decays exponentially for large values of Ω because the realization of high blueshift $\alpha |P^2|$ is unlikely. Moreover, frequencies $\omega < \omega_X$ are not possible since interactions are repulsive and lead to an increase of energy only. Equation (22) demonstrates that in the regime of high pumping the oscillator spectrum is strongly asymmetric and broadened due to fluctuations of the resonance frequency.

For an arbitrary value of pumping strength the general analytical result for the oscillator spectrum can be obtained by means of the Fokker–Planck equation technique [28, 45], similarly to the case of the noise-driven Duffing oscillator [46]. The spectrum reads

$$\langle |P(\omega)^2| \rangle \propto \mathrm{Im} \sum_{n=0}^{\infty} \frac{(I_n)^2}{\lambda_n - \omega}, \tag{23}$$

where

$$\lambda_n = \omega_X + \mathrm{i}\frac{\Gamma_X}{2} - 2\mathrm{i}(n+1)\sqrt{\left(\frac{\Gamma_X}{2}\right)^2 + \mathrm{i}\alpha S},$$

$$I_n = \frac{4b\sqrt{(n+1)a}}{(a+b)^2} \left(\frac{a-b}{a+b} \right)^n, \quad a = \frac{\Gamma_X}{S}, \quad b = \sqrt{a^2 + \frac{4\mathrm{i}\alpha}{S}}.$$

In the linear in the pumping regime where $S \to 0$ only the first term in the series equation (23) does not vanish and the result is reduced to a Lorentzian with FHWM equal to Γ_X. For a very large pumping, $\alpha \langle |P^2| \rangle \gg \Gamma_X$, the series reduce to equation (22).

The spectra of the single oscillator, $\langle |P(\omega)|^2 \rangle$, calculated for different pumping strengths are shown in figure 1(b). The spectrum at the strong pumping represented by a red/solid curve is strongly broadened and shifted as compared with the spectrum found in the linear regime. The latter is shown by a black/dashed black curve. The width of the nonlinear spectrum is of the same order as the blueshift. The spectrum found by the stochastic linearization, equation (22), and shown by a red/dotted curve in figure 1(b) approximates well the exactly calculated one, equation (23). The strong asymmetry of emission spectra calculated for the nonlinear regime is clearly seen from the figure.

This concludes the discussion of the single oscillator and we now proceed to the analysis of the quantum dot coupled with the cavity mode.

4.2. A single dot coupled with the cavity

To start with, we recall that in the linear in the pumping regime, $S \to 0$, and under the conditions of the strong coupling, $g \gg \Gamma_C, \Gamma_X$, the spectrum described by equation (8) with $N = 1$ consists of two distinct peaks at the frequencies of the system eigenmodes, excitonic polaritons. The main question we address here is how this two-peak spectrum changes with allowance for the nonlinearity. In the general case the emission spectrum under strong pumping should be
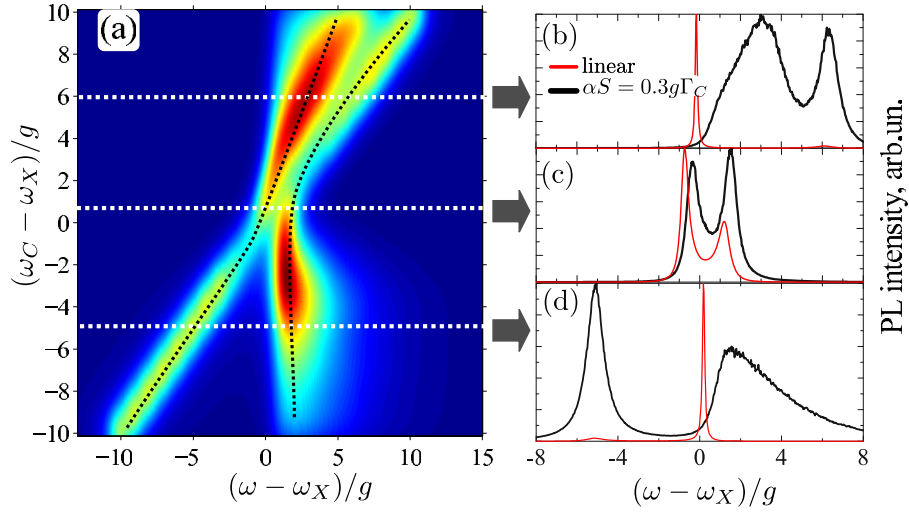
Figure 2. (a) Photoluminescence spectra for a single quantum dot coupled to the microcavity mode as a function of the detuning between cavity and exciton frequencies. Panels (b), (c) and (d) show the spectra for $\omega_C = \omega_X + 6g$, $\omega_C = \omega_X + 0.5g$ and $\omega_C = \omega_X - 5g$, respectively. Black/thick and red/thin lines in panels (b), (c) and (d) correspond to the nonlinear and linear in the pumping regime, $\alpha S = 0.3g\Gamma_C$ and $S = 0$, respectively. These curves are normalized to their maximum values. Black/dashed curves in panel (a) are a guide to the eye demonstrating anticrossing. Calculations are performed at $\Gamma_X = 0.1g$, $\Gamma_C = g$, $\alpha S = 0.3g\Gamma_C$. The time-domain integration was performed up to $t = 100g^{-1}$, with the time step $0.003g^{-1}$; the spectra were averaged over ensemble with 4000 realizations of random forces.

calculated numerically. This can be done either by reducing the problem to the Fokker–Planck equation [45] or directly integrating the set of equations (3). The latter procedure turns out to be more efficient, because the Fokker–Planck equation is computationally demanding already for $N = 1$ due to the large number of independent variables. In our calculations, we have used the simplest 1.5-order Heun method for the integration of stochastic differential equations [47, 48].

Luminescence spectra calculated for different detunings between the exciton and photon modes are presented in figure 2. Panel (a) shows the color plot of the emission intensity. Panels (b), (c) and (d) present the spectra for the detuning $\omega_C - \omega_X$ equal to $6g$, $0.5g$ and $-5g$, respectively. Thin/red and thick/black curves are calculated, respectively, for (i) the linear regime $S \to 0$ and (ii) the regime where the nonlinearity is already strong, $S = 0.3\Gamma_C/\alpha$. The spectra are normalized to their maximum values, and the other parameters of the calculations are given in the caption to the figure. The calculation demonstrates that the nonlinear spectra retain the characteristic two-peak structure, although the spectral shape is strongly affected by the nonlinearity; in particular, it becomes asymmetric, as clearly seen in figures 2(b) and (d). The spectral maxima in the nonlinear regime clearly exhibit anticrossing behavior, see figure 2(a). From this, we conclude that the strong coupling survives even for the nonlinear regime if $\alpha \langle |P^2| \rangle \lesssim g$.

Let us now discuss the spectra in figure 2 in more detail. We start with the case of large detuning between exciton and photon modes, $|\omega_X - \omega_C| \gg g$. In this situation the spectrum
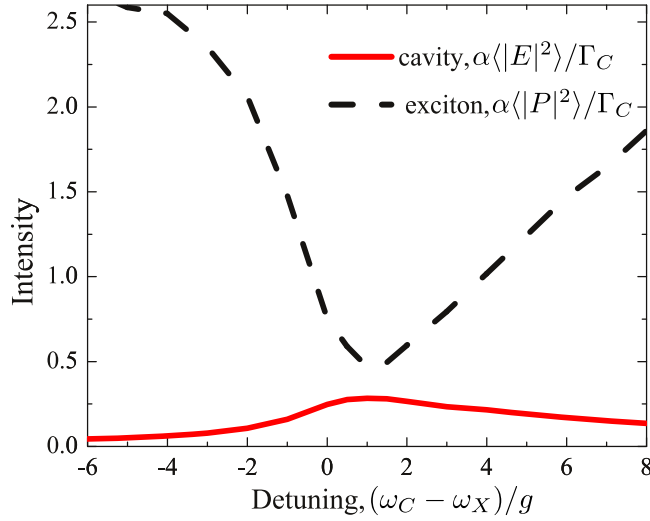
Figure 3. Intensities of photon and exciton modes as functions of the detuning $\omega_C - \omega_X$. Red/solid and black/dashed curves correspond to $\alpha\langle|E|^2\rangle/\Gamma_C$ and $\alpha\langle|P|^2\rangle/\Gamma_C$, respectively. The parameters of calculations are the same as in figure 2.

has two peaks related to the cavity and exciton emission. It is noteworthy that in the nonlinear regime, the blueshift of the exciton is determined by the dot population which, in turn, is related to the detuning: $\langle|P|^2\rangle \approx S(\omega_X - \omega_C)^2/(\Gamma_C g^2)$ (provided that $\Gamma_X \ll \Gamma_C$ and $\Gamma_C \ll |\omega_X - \omega_C|$). Hence, if bare exciton frequency ω_X is fixed, but the cavity frequency ω_C is varied, the position of the exciton peak changes due to the variation of the blueshift.

To confirm this argument, we have plotted in figure 3 the dependence of the stationary intensities $\langle|E|^2\rangle$ and $\langle|P^2|\rangle$ on the detuning. For large detuning one has $\langle|P^2|\rangle \gg \langle|E|^2\rangle$, which is explained by the longer exciton lifetime as compared with the photon lifetime, $\Gamma_C \gg \Gamma_X$. For small values of detuning the curves become closer to each other as a result of the coupling between exciton and photon modes.

Another important feature revealed in figure 2 is the strong asymmetry between the spectral shapes of the exciton peak for large positive and negative detuning, cf figures 2(b) and (c). This is quite different from the linear regime, where the spectra equation (8) are symmetric with respect to zero detuning. In the nonlinear case the exciton peak is asymmetrically broadened due to the frequency fluctuations, like in the case of a single oscillator, and the shape of the broadened peak depends on the sign of detuning. For negative detuning, $\omega_C - \omega_X < 0$, the high-energy tail dominates the spectrum similarly to the case of the dot decoupled from the cavity, see section 4.1 and figure 1(b), while for positive detuning, $\omega_C - \omega_X > 0$, this tail is quenched. This is related to the fact that strong fluctuations of exciton polarization P are suppressed since they correspond to large blueshifts where the exciton mode approaches the cavity mode and, hence, short lifetimes.

To understand this effect in depth, we have plotted in figure 4 the emission spectra ((a), (b)) along with the distribution functions of the quantum dot exciton intensity $|P|^2$. Distribution functions $p(|P|^2)$, shown by black/solid curves in figures 4(c) and (d), were extracted from the numerical solutions of the system (8). For comparison, red/dashed curves show exponential distributions (20) with the same average values of $|P|^2$. The emission
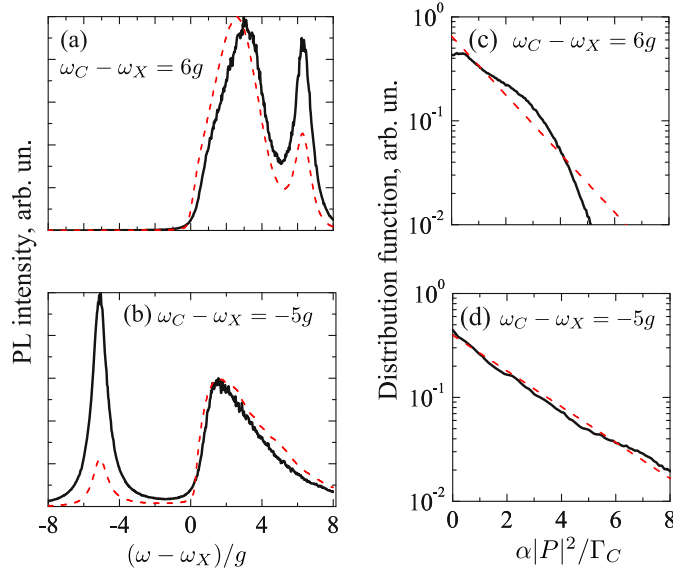
Figure 4. (a), (b) Cavity emission spectra calculated for the detuning $\omega_C - \omega_X = 6g$ (a) and $\omega_C - \omega_X = -5g$ (b). (c), (d) Distribution functions of the intensity $|P|^2$ calculated for the same parameters as in panels (a) and (b), respectively. Black/solid lines represent the results of direct numerical calculation, and red/dashed lines are calculated according to equations (20) and (24). Other parameters of calculations are the same as in figure 2.

spectrum of the microcavity can be presented in the following phenomenological form similar to equations (13) and (16) obtained in the stochastic linearization method:

$$I(\omega) \propto \int d\Omega F(\Omega) I_{\text{lin}}(\omega), \tag{24}$$

where $I_{\text{lin}}(\omega)$ is given by equation (8) with $\omega_X = \Omega$ and the distributions $F(\Omega)$ and $p(|P^2|)$ are related by equation (18). The corresponding spectra, calculated with numerically found functions $p(|P|^2)$, are shown in figures 4(a) and (b) by red/thin curves. We see that equation (24) satisfactorily describes the shape of the exciton peaks for both signs of the detuning and clearly demonstrates the correspondence between the shape of the exciton peak and the distribution function of the intensity $|P|^2$. For negative detuning the distribution function and the excitonic peak have exponential tails, similarly to the case of a single oscillator, equation (22). Suppression of this tail for positive detuning means that the distribution function decays faster than exponential (cf red and black curves in figure 4(c)), which is explained by the interaction of excitonic and photonic modes. Indeed, for $\omega_C > \omega_X$ the nonlinear blueshift of the exciton frequency decreases the detuning. Consequently, the exciton lifetime becomes effectively smaller due to the Purcell effect which suppresses the probability of such a large detuning. Another effect leading to the same result is the repulsion of the excitonic mode with high blueshift from the cavity mode. In the opposite case, $\omega_C < \omega_X$, the absolute value of the detuning is further increased by the blueshift, so the shape of the excitonic peak is not modified by the interaction with the cavity.

Phenomenological equation (24) fails, however, to reproduce the ratio between the magnitudes of the excitonic and photonic peaks in the spectra. Formally, equation (24) is valid
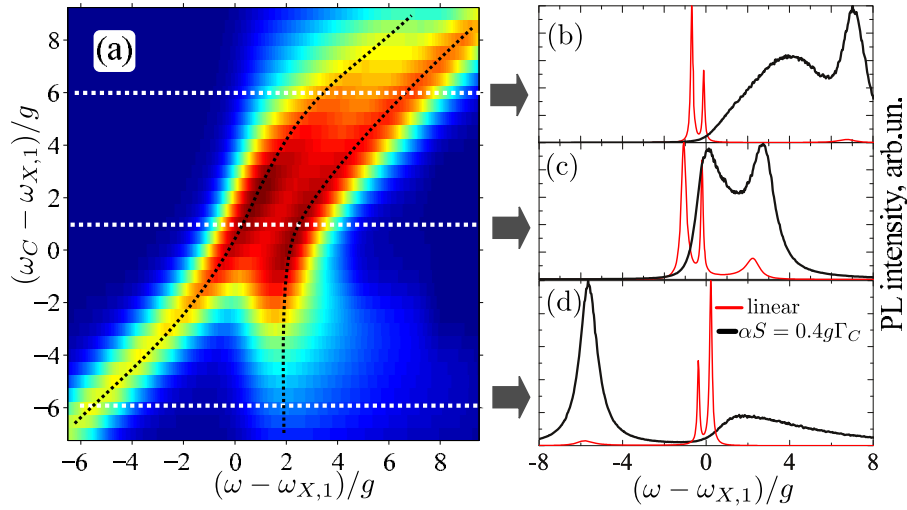
Figure 5. (a) Photoluminescence spectra for two quantum dots coupled to microcavity mode as function of the detuning between cavity and exciton dot. Panels (b), (c) and (d) show the spectra for $\omega_C = \omega_{X,1} + 6g$, $\omega_C = \omega_X + g$, $\omega_C = \omega_X - 6g$, respectively. Black/thick and red/thin lines in panels (b)–(d) correspond to nonlinear and linear in pumping regime, $\alpha S = 0.4g\Gamma_C$ and $S \to 0$, respectively. These curves are normalized at their maximum values. Black/dashed curves in panel (a) are guides for the eye demonstrating anti-crossing. Calculation was carried out for $\omega_{X,1} - \omega_{X,2} = g$, other parameters are the same as in figure 2.

provided that the timescale of the fluctuations of P is large compared with other timescales in the system (cf equation (14)) or the magnitude of the blueshift exceeds by far all other energy scales. Neither of these conditions holds in the system under study.

4.3. Two dots coupled with the cavity

Now we turn to the discussion of the emission spectra of the cavity with two embedded dots, shown in figure 5. A specific feature of this problem in the linear regime is the formation of the collective, superradiant mode of quantum dot excitons [17, 18, 28]. In particular, as discussed above in section 2, there are three eigenmodes of the homogeneous linear system equation (3) for $N = 2$. In the case where $\omega_{X,i} = \omega_{X,2}$, one of these modes, with the excitons oscillating with the opposite phases, $P_1 = -P_2$, does not interact with the cavity mode; it is called dark. Two remaining modes correspond to the excitons, oscillating in phase, $P_1 = P_2$, and are formed by the coupling between the superradiant mode of the excitons and the cavity mode. Only two peaks are manifested in the emission spectrum. The effect leads to an enhancement of the Rabi splitting between these peaks from g to $\sqrt{N}g$, see equation (8). When the frequencies of the dots $\omega_{X,i}$ are different or the exciton tunneling between the dots is introduced, the dark modes mix with the superradiant mode and the spectrum acquires a three-peak shape. As was demonstrated in previous work [18], the superradiant mode is stable against disorder when the characteristic splitting of the dot frequencies is less than $g\sqrt{N}$. Here, we analyze the stability of the superradiant mode against the interactions.

Figure 5 shows the emission spectra of the microcavity containing two quantum dots for various frequencies of the cavity mode. The frequency separation between the dots was fixed to be $\omega_{X,2} - \omega_{X,1} = g$ and the ω_C was varied. The overall intensity dependence on the emission and cavity frequency shown in figure 5(a) is quite similar to the intensity distribution for one dot in the microcavity (see figure 2(a)) and clearly demonstrates two peaks for any given cavity mode position. Thus, the superradiant mode is stable against the interaction.

Panels (b), (c) and (d) of figure 5 present the details of emission spectra for three different cavity mode positions. Black/solid curves are calculated for the strong pumping where the nonlinear behavior is pronounced and red/thin curves correspond to the linear regime. The emission spectra in the nonlinear regime corresponding to rather large detunings (panels (b) and (d)) demonstrate the asymmetry studied for the single dot in the cavity in section 4.2. Interestingly, the spectra in the linear regime demonstrate three peaks: two stronger ones correspond to the dot emission and a weaker one to the cavity emission. The presence of nonlinearity induced by the strong pumping qualitatively changes the emission spectrum: excitonic peaks merge and their intensity drops. Note, however, that the strong coupling regime is still maintained, see anticrossing in figure 5. The smallest splitting between the maxima of the spectra is larger than the Rabi splitting for the single dot $2g$. This is a fingerprint of the superradiant mode stability in the nonlinear regime.

Thus, the superradiant mode becomes stabilized by interactions. Indeed, for positive detunings, $\omega_C > \omega_{X,1}, \omega_{X,2}$, the blueshifts of the quantum dots are different: the dot with higher exciton frequency (dot 2 in our calculation) has smaller lifetime due to proximity to the cavity mode, correspondingly, smaller exciton intensity $\langle |P_2|^2 \rangle < \langle |P_1|^2 \rangle$ and, hence, smaller blueshift. Hence, with an increase of the pumping rate the blueshifted dot frequencies approach each other, resulting in a decrease of the splitting between exciton frequencies and stabilization of the superradiant mode.

5. Conclusions

To conclude, we have developed a theory of nonlinear emission of large quantum dots coupled to the optical mode of the microcavity under non-resonant excitation. We model quantum dot excitons as nonlinear oscillators taking into account the repulsive exciton–exciton interactions both within the dot and between the quantum dot and excitonic reservoir. We use the random sources approach to model the relaxation processes, and apply stochastic linearization and numerical integration of the Langevin equations to determine the spectra.

Our model clearly shows that interactions (i) blueshift the transition energy and (ii) to the same extent broaden the emission peak. The interactions result in a complex behavior of the exciton lifetimes and intensities of emission as functions of pumping rate. The emission lines are strongly asymmetric and bear information on the exciton statistics. Contrary to the linear regime, the lineshapes are sensitive to the sign of the detuning between the exciton and photon modes. Interestingly, even for substantial pumping the strong coupling regime between the cavity mode and the quantum dot exciton can be preserved. Moreover, if two quantum dots are placed in the cavity, the superradiant behavior can be stabilized by the pumping.

IOP Institute of Physics **Φ** DEUTSCHE PHYSIKALISCHE GESELLSCHAFT

Acknowledgments

References

[1] Ivchenko E L 2005 *Optical Spectroscopy of Semiconductor Nanostructures* (Harrow, UK: Alpha Science International)
[2] Bayer M, Stern O, Hawrylak P, Fafard S and Forchel A 2000 *Nature* **405** 923–6
[3] Reithmaier J P, Sek G, Löffler A, Hofmann C, Kuhn S, Reitzenstein S, Keldysh L V, Kulakovskii V D, Reinecke T L and Forchel A 2004 *Nature* **432** 197
[4] Yoshie T, Scherer A, Hendrickson J, Khitrova G, Gibbs H M, Rupper G, Ell C, Shchekin O B and Deppe D G 2004 *Nature* **432** 200
[5] Peter E, Senellart P, Martrou D, Lemaitre A, Hours J, Gérard J M and Bloch J 2005 *Phys. Rev. Lett.* **95** 067401
[6] Agranovich V and Ginzburg V 1984 *Crystal Optics with Spatial Dispersion and Excitons* (*Springer Series in Solid-State Sciences*) (Berlin: Springer)
[7] Kavokin A and Malpuech G 2003 *Cavity Polaritons* (Amsterdam: Elsevier)
[8] Kavokin A, Baumberg J, Malpuech G and Laussy F 2006 *Microcavities* (Oxford: Clarendon)
[9] Rashba E and Sturge M (ed) 1982 *Excitons* (*Modern Problems in Condensed Matter Science* vol 2) (Amsterdam: North-Holland)
[10] Khitrova G, Gibbs H M, Kira M, Koch S W and Scherer A 2006 *Nature Phys.* **2** 81
[11] Kasprzak J, Reitzenstein S, Muljarov E A, Kistner C, Schneider C, Strauss M, Höfling S, Forchel A and Langbein W 2010 *Nature Mater.* **9** 304
[12] Nomura M, Kumagai N, Iwamoto S, Ota Y and Arakawa Y 2010 *Nature Phys.* **6** 279–83
[13] Calic M *et al* 2011 *Phys. Rev. Lett.* **106** 227402
[14] Dousse A, Suffczynski J, Beveratos A, Krebs O, Lemaitre A, Sagnes I, Bloch J, Voisin P and Senellart P 2010 *Nature* **466** 217
[15] Ota Y, Iwamoto S, Kumagai N and Arakawa Y 2011 *Phys. Rev. Lett.* **107** 233602
[16] Tandaechanurat A, Ishida S, Guimard D, Nomura M, Iwamoto S and Arakawa Y 2011 *Nature Photon.* **5** 91–4
[17] Keldysh L V, Kulakovskii V D, Reitzenstein S, Makhonin M N and Forchel A 2007 *JETP Lett.* **84** 494
[18] Averkiev N S, Glazov M M and Poddubnyi A N 2009 *J. Exp. Theor. Phys.* **108** 836
[19] Khitrova G, Gibbs H M, Jahnke F, Kira M and Koch S W 1999 *Rev. Mod. Phys.* **71** 1591–639
[20] Deych L I, Erementchouk M V, Lisyansky A A, Ivchenko E L and Voronov M M 2007 *Phys. Rev.* B **76** 075350
[21] Kasprzak J *et al* 2006 *Nature* **443** 409
[22] Malpuech G, Solnyshkov D D, Ouerdane H, Glazov M M and Shelykh I 2007 *Phys. Rev. Lett.* **98** 206402
[23] Butov L V, Lai C W, Ivanov A L, Gossard A C and Chemla D S 2002 *Nature* **417** 47
[24] Timofeev V B, Gorbunov A V and Demin D A 2011 *Low Temp. Phys.* **37** 179
[25] Aspelmeyer M, Gröblacher S, Hammerer K and Kiesel N 2010 *J. Opt. Soc. Am.* B **27** A189
[26] Laussy F P, Glazov M M, Kavokin A, Whittaker D M and Malpuech G 2006 *Phys. Rev.* B **73** 115343
[27] del Valle E, Laussy F P and Tejedor C 2009 *Phys. Rev.* B **79** 235326
[28] Poddubny A N, Glazov M M and Averkiev N S 2010 *Phys. Rev.* B **82** 205330
[29] Andreani L C, Panzarini G and Gérard J M 1999 *Phys. Rev.* B **60** 13276
[30] Kaliteevski M A, Brand S, Abram R A, Nikolaev V V, Maximov M V, Sotomayor Torres C M and Kavokin A V 2001 *Phys. Rev.* B **64** 115305
[31] Glazov M, Ivchenko E, Poddubny A and Khitrova G 2011 *Phys. Solid State* **53** 1753
[32] Houdré R, Stanley R P and Ilegems M 1996 *Phys. Rev.* A **53** 2711–5

IOP Institute of Physics ⬥ DEUTSCHE PHYSIKALISCHE GESELLSCHAFT

[33] Albert F *et al* 2012 arXiv:1206.0592

[34] Parascandolo G and Savona V 2005 *Phys. Rev.* B **71** 045335

[35] Scheibner M, Schmidt T, Worschech L, Forchel A, Bacher G, Passow T and Hommel D 2007 *Nature Phys.* **3** 106–10

[36] Khitrova G and Gibbs H M 2007 *Nature Phys.* **3** 84–6

[37] Kasprzak J, Patton B, Savona V and Langbein W 2011 *Nature Photon.* **5** 123

[38] Kozub M, Pawicki L and Machnikowski P 2012 *Phys. Rev.* B **86** 121305

[39] Tosi G, Christmann G, Berloff N G, Tsotsis P, Gao T, Hatzopoulos Z, Savvidis P G and Baumberg J J 2012 *Nature Phys.* **8** 190–4

[40] Wouters M and Savona V 2009 *Phys. Rev.* B **79** 165302

[41] Sarchi D, Wouters M and Savona V 2009 *Phys. Rev.* B **79** 165315

[42] Wouters M and Savona V 2010 *Phys. Rev.* B **81** 054508

[43] Budgor A B 1976 *J. Stat. Phys.* **15** 355

[44] Spanos P, Kougioumtzoglou I and Soize C 2011 *Probab. Eng. Mech.* **26** 10

[45] Risken H 1989 *The Fokker–Planck Equation: Methods of Solution and Applications* (Berlin: Springer)

[46] Dykman M I and Krivoglaz M A 1980 *Physica* A **104** 495–508

[47] Kloeden P and Platen E 2010 *Numerical Solution of Stochastic Differential Equations* (*Stochastic Modelling and Applied Probability*) (Berlin: Springer)

[48] Burrage K, Lenane I and Lythe G 2007 *SIAM J. Sci. Comput.* **29** 245